UDK 67.017:544.344.016.2:549.641
Original scientific article/Izvirni znanstveni članek

ISSN 1580-2949
MTAEC9, 52(1)51(2018)

NOVEL MATERIALS BASED ON $La_{0.75}Sr_xA_{0.25-x}Cr_{0.5}Mn_{0.5}O_3$ (A=Ba, Ca, Mg) AS FULL-CERAMICS ANODES IN HIGH-TEMPERATURE FUEL CELLS

NOVI MATERIALI NA OSNOVI $La_{0.75}Sr_xA_{0.25-x}Cr_{0.5}Mn_{0.5}O_3$ (A=Ba, Ca, Mg) KOT KERAMIČNE ANODE V VISOKOTEMPERATURNIH GORIVNIH CELICAH

Tina Skalar, Marjan Marinšek, Klementina Zupan

Faculty of Chemistry and Chemical Technology, Večna pot 113, 1000 Ljubljana
klementina.zupan@fkkt.uni-lj.si

Prejem rokopisa – received: 2017-07-17; sprejem za objavo – accepted for publication: 2017-09-08

doi:10.17222/mit.2017.120

Among alternative anode materials for high-temperature fuel cells, the complex ceramic oxide $La_{0.75}Sr_{0.25}Mn_{0.5}Cr_{0.5}O_3$ (LSCM) has recently shown good catalytic activity regarding fuel oxidation and sufficient stability in reductive environments at relatively low steam-to-carbon ratios. However, the electrical and ionic conductivities of LSCM are lower compared to some other perovskite materials. One of the possibilities to improve the conductivity of LSCM is in its composition variations, i.e., altering the Sr-content, doping on the A-site of the perovskite with other ions (Ba, Ca and Mg), and varying the Mn-to-Cr ratio on the B-site of the perovskite. In this paper, systems with the general formula $La_{0.75}Sr_xA_{0.25-x}Cr_{0.5}Mn_{0.5}O_3$ (A = Ba, Ca, Mg, x varies between 0 and 0.25) are described. Within the investigated system, prepared materials after synthesis contain the perovskite structure as a main crystallographic phase with relatively low additions of secondary phases. Any secondary phases are undesired, because they may substantially influence the electrical properties of the final materials. In samples with relatively high Sr-additions, a secondary Sr-rich phase Sr_2CrO_4 is also identified. Ca-doping may result in traces of $CaCr_2O_4$ phase in as-synthesized samples, while Ba-doping may lead to $BaCrO_4$ or $BaCO_3$ phases with higher Ba-additions. The quantity of the secondary phases may be controlled by calcination program or sintering conditions. Secondary phases, which may form additional grains or liquid phase, also influence the development of microstructures during sintering. Within the investigated compositions, the most promising materials are $La_{0.75}Sr_xCa_{0.25-x}Cr_{0.5}Mn_{0.5}O_3$ (x = 0.05–0.15), because they exhibit single-phase microstructure with fine grains after sintering at 1200 °C. Materials with Ba- or Mg-additions form precipitates of secondary phases at 1200 °C, which also remain present after sintering at higher temperatures.

Keywords: combustion synthesis, perovskite, thermal analysis, x-ray powder diffraction, quantitative microstructure analysis

$La_{0,75}Sr_{0,25}Mn_{0,5}Cr_{0,5}O_3$ (LSCM) je med alternativnimi anodnimi materiali za visokotemperaturne gorivne celice pokazal dobro katalitsko aktivnost za oksidacijo goriva ter zadovoljivo stabilnost v reduktivnih okoljih z relativno nizkim razmerjem med vodno paro in ogljikom. Vendar pa ima LSCM v primerjavi z nekaterimi drugimi perovskiti nekoliko nižjo električno in ionsko prevodnost. Ena od možnosti za izboljšanje njegove prevodnosti je v variacijah sestave, npr. sprememba koncentracije Sr, dopiranje na A mestu v perovskitu z drugimi ioni (Ba, Ca in Mg), variiranje razmerja med Mn in Cr na B mestu v perovskitu. V prispevku obravnavamo sistem s splošno formulo $La_{0.75}Sr_xA_{0.25-x}Cr_{0.5}Mn_{0.5}O_3$ (A = Ba, Ca, Mg, x variira med 0 in 0,25). Materiali v preiskovanem sistemu po sintezi kot glavno fazo vsebujejo perovskit z relativno nizko vsebnostjo sekundarnih faz. Kakršnekoli sekundarne faze so nezaželene, ker lahko bistveno vplivajo na električne lastnosti končnih materialov. V vzorcih z relativno visokim dodatkom stroncija smo identificirali s stroncijem bogato fazo Sr_2CrO_4. Dopiranje s kalcijem se v vzorcih po sintezi lahko odrazi v nastanku faze $CaCr_2O_4$, medtem ko dopiranje z barijem pri višjih koncentracijah lahko vodi v nastanek $BaCrO_4$ ali $BaCO_3$. Na vsebnost sekundarnih faz lahko vplivamo s pogoji kalcinacije oziroma sintranja. Sekundarne faze, ki med toplotno obdelavo vzorca tvorijo dodatna zrna ali tekočo fazo, vplivajo na razvoj mikrostrukture med sintranjem. Med preiskovanimi sestavami, so najbolj perspektivni materiali $La_{0.75}Sr_xCa_{0.25-x}Cr_{0.5}Mn_{0.5}O_3$ (x = 0,05 – 0,15), ker imajo enofazno mikrostrukturo že po sintranju pri 1200 °C. Sestave z dodatki Ba ali Mg pa pri 1200 °C vsebujejo izločke sekundarnih faz, ki v mikrostrukturi ostanejo tudi po sintranju pri višjih temperaturah.

Ključne besede: analiza zgorevanja, perovskit, termična analiza, rentgenska difrakcija prahu, kvantitativna analiza mikrostrukture

1 INTRODUCTION

Among fuel cells, their high-temperature form is the most efficient (>70 % with fuel regeneration) for gaseous fuels' conversion directly into electrical power and one of the cleanest way to produce electricity due to their low greenhouse-gas emissions.[1–3] However, the performance and stability of a SOFC are critically dependent on the activity and structural stability of various cell components, including the electrolyte, anode, cathode, and interconnect. The most significant technical barriers currently addressed relate to anode and cathode.[4] Conventionally used materials for the anodes in ceramic fuel cells are Ni/YSZ composite materials, due to their high electrical conductivity and electro-chemical activity for fuel oxidation reaction. Nevertheless, Ni has several weaknesses, among others a tendency to coke in a hydrocarbon environment and irreversible poisoning of the catalyst by sulphur.[5] The major challenges in the selection of these types of fuel-cell anodes include the poisoning issue and carbon deposition,[6] surface diffusion of adsorbed reactant gases and charge transfer at the

electrode-pore phase boundary. Regarding the development of the anode material, it is essential to be able to engineer the mass and charge-transfer through the bulk through the development of appropriate, efficient processing and fabrication techniques.

Conductive oxides including perovskites with nominal formula $La_xSr_{1-x}Mn_{0,5}Cr_{0,5}O_{3-\delta}$ (LSCM) are known to have reasonable catalytic activity towards the oxidation of hydrogen and methane, in addition to the good coke tolerance and improved sulphur-poisoning resistance.[7] Lanthanum substitution in lanthanum chromite oxides by alkali earth elements (specifically Ca, Sr, and Ba) significantly affects their electrochemical performance.[8,9] The redox stability of doped chromites is probably due to the high chemical stability of Cr^{3+} at the B-site of the perovskite among the first-row transition-metal system (Cr^{3+}>Fe^{3+}>Mn^{3+}>Co^{3+}).[10,11] According to Deleebeeck and co-authors, the elimination of Sr in $La_{1-x}Sr_xMn_{1-y}Cr_yO_{3\pm\delta}$ improves electronic conductivity in a wet hydrogen atmosphere and also enhances thermochemical stability.[12] Relatively high strontium content (x = 0.2) also results in poorer catalytic activity, while catalytic activity towards hydrogen oxidation improves with increasing manganese content (y = 0.4 – 0.6).[13] Therefore, the question of an optimal perovskite material composition remains open. Microstructure development and final electrical properties strongly depend on the presence of isolative secondary phases formed in perovskite during the preparation process and/or subsequent sintering. Several routes are possible to prepare complex oxide powders, including solid-state reaction,[14] the chelating method,[15] gel casting,[16] and co-precipitation[17]. Among the various preparation techniques, combustion synthesis[18–21] enables the preparation of ultrafine soft agglomerated metal oxide powder. The secondary phase present after synthesis can be controlled by subsequent calcination.

In the present contribution, materials with mixed doping at the A site of the perovskite by earth alkali elements were prepared for the first time. A series of complex metal oxide materials with general formula $La_{0.75}Sr_xA_{0.25-x}Cr_{0.5}Mn_{0.5}O_3$ (A = Ba, Ca, Mg, x varies between 0 and 0.25) were prepared by combustion synthesis. The thermal behaviour of the citrate-nitrate gels was determined with thermogravimetric analyses. After synthesis, samples were pressed into pellets and sintered at different temperatures. The crystalline phase formation was followed by X-ray powder diffraction and the relationship between the presence of the secondary phase in the complex metal oxide and microstructure development was studied in relation to output chemical composition.

2 EXPERIMENTAL PART

Samples with the nominal composition $La_{0.75}Sr_xA_{0.25-x}Cr_{0.5}Mn_{0.5}O_3$ (A = Ba, Ca, Mg, x varies between 0 and 0.25) were prepared by modified citrate-nitrate combustion reaction (**Table 1**). Stoichiometric amounts of metal nitrates $La(NO_3)_3{\cdot}6H_2O$, $Sr(NO_3)_2$, $Ca(NO_3)_2$, $Mg(NO_3)_2$, $Ba(NO_3)_2$, $Cr(NO_3)_3{\cdot}9H_2O$ and $Mn(NO_3)_2{\cdot}4H_2O$ and citric acid (analytical reagent grade) were dissolved with minimum quantities of water. Five or six reactant solutions were mixed to form a reaction solution and then preserved at 60 °C under vacuum (p = 5–7 mbar) until it transformed into a gel reactive mixture (at least 6 hours). The citrate/nitrate molar ratios in the starting solutions were 0.18, respectively. After water evaporation, the gel was then slightly crushed in an agate mortar and uni-axially pressed into pellets (Φ = 12 mm, h = 30 mm, p = 17 MPa). These samples were placed on a corundum plate and ignited at the top of the pellet with a hot tip to start an auto-ignition reaction that travels as a reaction zone throughout the pellet. During the exothermic combustion reaction, high temperatures are reached in a very short reaction time, yielding a fine-powdered product.

Table 1: Compositions, sample notations and secondary phase present in *as prepared* samples

Sample composition	Sample name	Secondary phase in *as prepared* sample
$La_{0.75}\mathbf{Mg_{0.25}}Sr_0Cr_{0.5}Mn_{0.5}O_3$	Mg25Sr0	/
$La_{0.75}\mathbf{Mg_{0.20}}Sr_{0.05}Cr_{0.5}Mn_{0.5}O_3$	Mg20Sr5	Sr_2CrO_4
$La_{0.75}\mathbf{Mg_{0.15}}Sr_{0.10}Cr_{0.5}Mn_{0.5}O_3$	Mg15Sr10	Sr_2CrO_4
$La_{0.75}\mathbf{Mg_{0.10}}Sr_{0.15}Cr_{0.5}Mn_{0.5}O_3$	Mg10Sr15	Sr_2CrO_4
$La_{0.75}\mathbf{Mg_{0.05}}Sr_{0.2}Cr_{0.5}Mn_{0.5}O_3$	Mg5Sr20	Sr_2CrO_4
$La_{0.75}\mathbf{Ca_{0.25}}Sr_0Cr_{0.5}Mn_{0.5}O_3$	Ca25Sr0	$CaCrO_4$
$La_{0.75}\mathbf{Ca_{0.20}}Sr_{0.05}Cr_{0.5}Mn_{0.5}O_3$	Ca20Sr5	/
$La_{0.75}\mathbf{Ca_{0.15}}Sr_{0.10}Cr_{0.5}Mn_{0.5}O_3$	Ca15Sr10	/
$La_{0.75}\mathbf{Ca_{0.10}}Sr_{0.15}Cr_{0.5}Mn_{0.5}O_3$	Ca10Sr15	Sr_2CrO_4
$La_{0.75}\mathbf{Ca_{0.05}}Sr_{0.20}Cr_{0.5}Mn_{0.5}O_3$	Ca5Sr20	Sr_2CrO_4
$La_{0.75}\mathbf{Ba_{0.25}}Sr_0Cr_{0.5}Mn_{0.5}O_3$	Ba25Sr0	$BaCrO_4$,
$La_{0.75}\mathbf{Ba_{0.20}}Sr_{0.05}Cr_{0.5}Mn_{0.5}O_3$	Ba20Sr5	$BaCO_3$
$La_{0.75}\mathbf{Ba_{0.15}}Sr_{0.10}Cr_{0.5}Mn_{0.5}O_3$	Ba15Sr10	Sr_2CrO_4
$La_{0.75}\mathbf{Ba_{0.10}}Sr_{0.15}Cr_{0.5}Mn_{0.5}O_3$	Ba10Sr15	Sr_2CrO_4
$La_{0.75}\mathbf{Ba_{0.05}}Sr_{0.20}Cr_{0.5}Mn_{0.5}O_3$	Ba5Sr20	Sr_2CrO_4
$\mathbf{La_{0.75}Sr_{0.25}Cr_{0.5}Mn_{0.5}O_3}$	**Sr25**	Sr_2CrO_4

The thermal behaviour (TG, DTG) of the reactive gels prior to the combustion was followed by thermogravimetric analyses (Netzsch STA 449 F3) at a heating rate of 10 K min^{-1}. The synthesized powders were milled in an agate mortar, un-axially pressed into pellets (100 MPa), and sintered at various temperatures (1200 °C, 1300 °C, 1400 °C and 1500 °C) for 1 h. The calcined and sintered samples were analysed with a PANalytical X'Pert PRO MPD apparatus. Data were collected in the range 2θ from 20° to 90° in steps of 0.033°. For the determination of the microstructure, the sintered tablets were polished (diamond pastes 3 μm and 0.25 μm), thermally etched, and subsequently analysed with an FE-SEM Zeiss ULTRA plus. The quantitative analyses of the microstructures were performed on digital images (the images were digitized into pixels with

255 different grey values) using Axiovision4.8 image-analysis software.

3 RESULTS AND DISCUSSION

The citrate-nitrate gel combustion described above is used as a technique for the preparation of complex metal oxides $La_{1-x}Sr_xA_{0.25-x}Mn_{0.5}Cr_{0.5}O_{3\pm\delta}$, in which the strontium at the A site is partly substituted by Ba, Ca, or Mg, and x varies between 0 and 0.25.

To obtain a better insight into the course of the citrate-nitrate combustion reaction of various reactive gels, a series of thermo-analytical tests is conducted (**Figure 1**). TG in combination with EGA may be used to study thermal stabilities of the reactive gel precursors and to unveil the reaction mechanism by determining volatile products of the citrate-nitrate combustion. It is evident that the citrate-nitrate combustion reaction proceeds over several consecutive steps. The first two intervals of mass losses (150–180 °C and 200–300 °C, respectively) are directly related to the citrate-nitrate combustion itself, as described in the literature.[22,23] This citrate-nitrate combustion is accompanied by the release of volatile products H_2O, CO_2, CO and NO and is very similar in all investigated systems. The third step of mass loss (300–380 °C) is a consequence of the so-called citrate after-burning, where some residual citrate reacts with oxygen from surrounding atmosphere. Peak temperatures of the first two intervals of mass losses differ slightly if Ba^{2+}, Ca^{2+} or Mg^{2+} ions are added to the original mixture of metal nitrates (La, Sr, Cr, and Mn) and citrate. It is well known from the literature that some metal ions (especially transition elements) exhibit a catalytic effect towards the citrate-nitrate combustion.[24,25] However, by comparing the TG curves of the investigated systems it appears that slight substitution of original metal ions with Ba^{2+}, Ca^{2+} or Mg^{2+} hinder the combustion reaction meaning that these three ions do not act catalytically. Solid residue (ash) above the citrate after-burning temperature is a mixture of nano-sized particles predominantly of the perovskite phase with minor additions of some secondary phases. These secondary phases (normally unreacted nitrates, formed carbonates or mixed oxides) are further decomposed or transformed during subsequent heating. In a combustion system, the subsequent heating occurs inside the combustion wave since citrate-nitrate combustion reaction provides temperatures around 1000 °C. During the investigated LSCM synthesis, very few secondary phases are formed. In contrast, additions of Ba^{2+}, Ca^{2+} or Mg^{2+} always resulted in the formation of secondary phases. After the addition of Ba^{2+} into the reactive precursor, the decomposition of a secondary phase may be found in temperature ranges 560–580 °C and 695–715 °C. Decomposition between 560–580 °C is accompanied by NO release, implying that some Ba^{2+} ions are not completely chelated with citrate but rather partially remain in the reactive gel as $Ba(NO_3)_2$. Subsequent decomposition between 695–715 °C is accompanied by O_2 release, which suggests that Ba-containing Ruddlesden–Popper phases are also formed during the combustion reaction. The addition of Ca^{2+} or Mg^{2+} ions into initial precursor mixtures after citrate-nitrate combustion causes the formation of some undesired Ca-containing or Mg-contain-

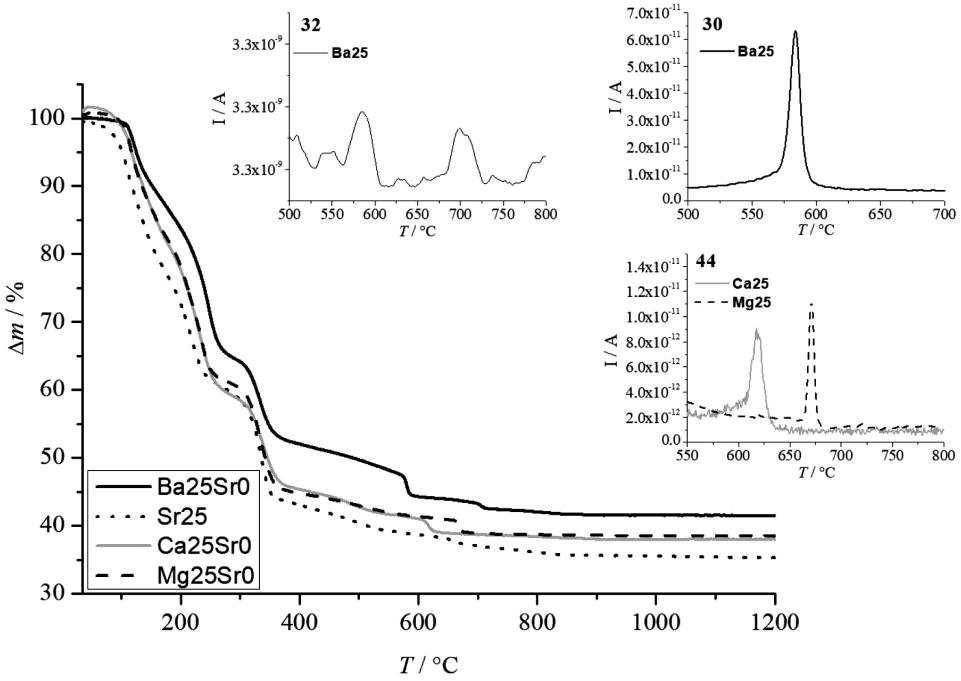

Figure 1: Thermal analysis of reactive gels (Ba25Sr0, Ca25Sr0, Mg25Sr0 and Sr25). Large graph represents mass losses; small graph inserts are QMS signals for 30, 32, and 44 fragments

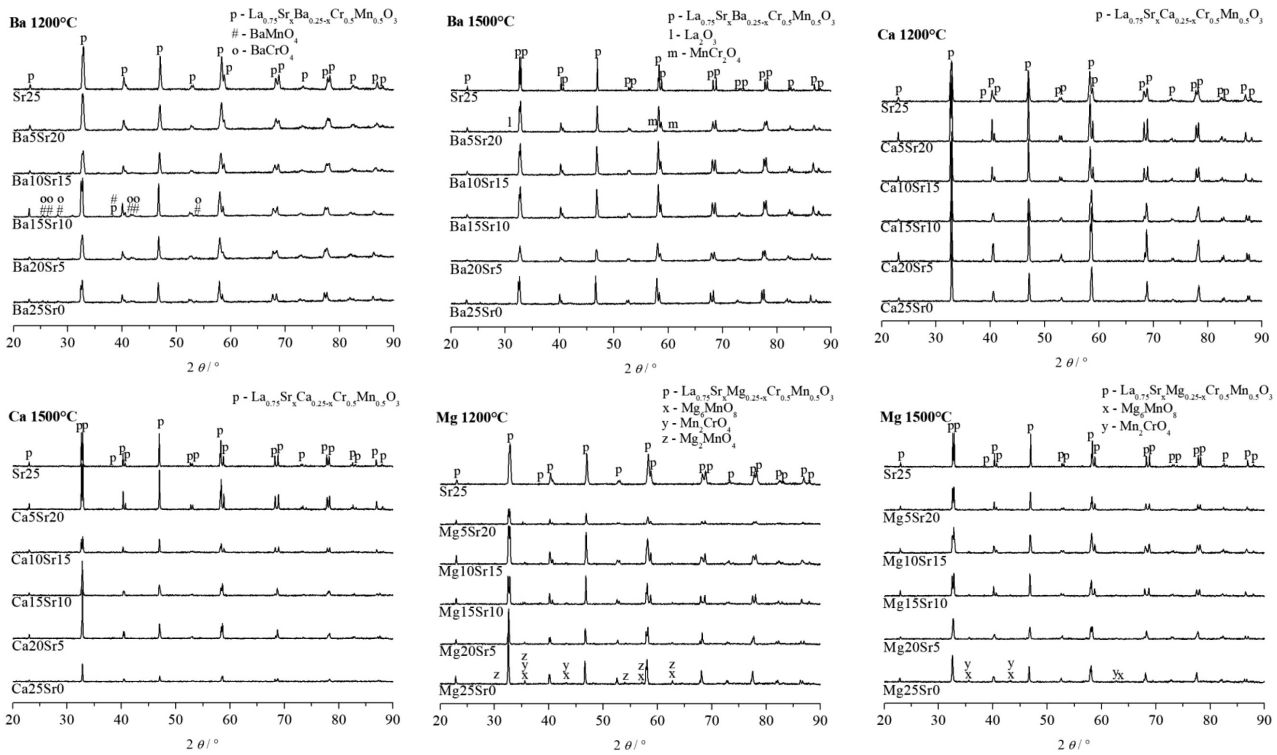

Figure 2: X-ray powder diffraction patterns of all samples after sintering at 1200 °C and 1500 °C

ing carbonates, which are decomposed through CO_2 release into mixed oxides at 595–630 °C or 655–675 °C, respectively. Thus, final *as prepared* ashes do not include metal nitrates or metal carbonates. Instead, other than the predominantly present perovskite phase, the *as prepared* samples may contain minor amounts of Ba-, Ca- or Mg-rich mixed oxides. Some of these secondary oxides are subsequently dissolved in the main perovskite phase during material sintering (LSMC or LSCCM systems); however, in the case of Ba- or Mg-doping inclusions of secondary phases are present also after sintering.

As-synthesized samples are not well crystalized and the main phase corresponded to perovskite crystal structure. In samples with relatively higher strontium content (x = 0.15 to 0.25), one of so-called Ruddlesden Popper phases Sr_2CrO_4 was detected. The formation of a stron-

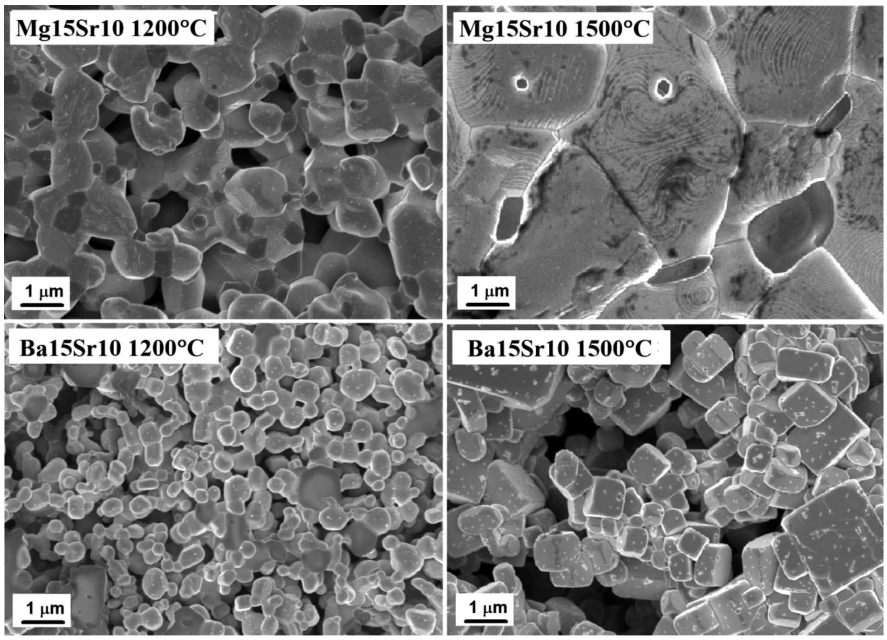

Figure 3: SEM micrographs of Mg15Sr10 and Ba15Sr10 after sintering at 1200 °C (left column) and after sintering at 1500 °C (right column)

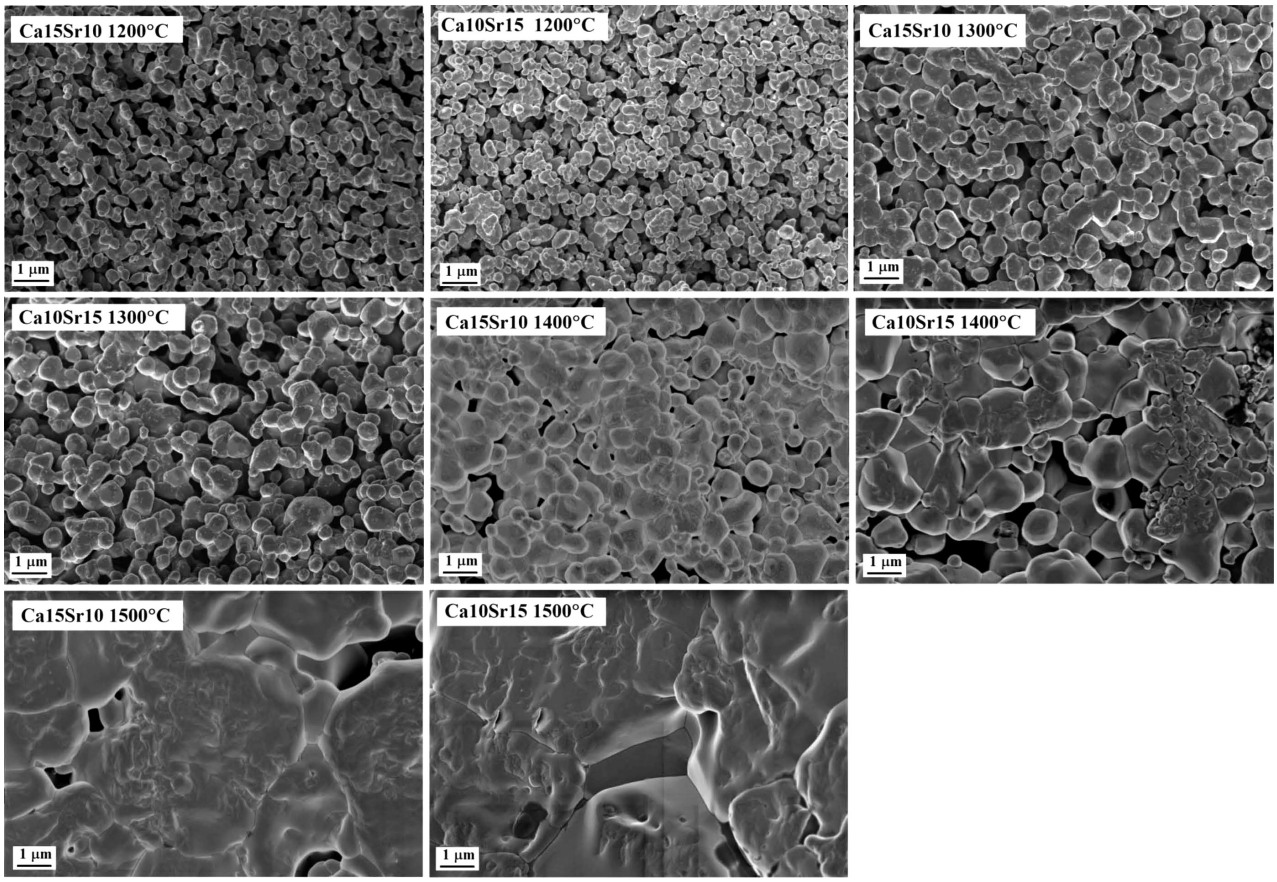

Figure 4: SEM micrographs of Ca15Sr10 (left column) and Ca10Sr15 (right column) samples sintered at 1200 °C, 1300 °C, 1400 °C, and 1500 °C

tium-rich secondary phase may be expected during synthesis in an oxygen-deficient atmosphere.[26] In samples Ba25Sr0 (x = 0) and Ba20Sr5 (x = 0.05), $BaCrO_4$, and $BaCO_3$ were identified respectively, while in sample Ca25Sr0 traces of $CaCrO_4$ were found. In samples containing magnesium, no secondary magnesium phases were detected after the synthesis.

After 1-hour sintering at various temperatures (in the range from 1200 °C to 1500 °C) in all samples, the perovskite phase turns out to be well crystallized. In all compositions containing magnesium (x = 0 to 0.20) after sintering at 1200 °C there are two possible secondary phases Mg_2MnO_4 and/or Mn_2CrO_4, and they remain in the samples after sintering as high as 1500 °C. In samples containing barium (x = 0 to 0.10) barium secondary phases $BaMnO_4$ and $BaCrO_4$ were found, indicating that higher calcination temperatures do not increase the solubility of Ba in $LaCrO_3$.[27] In samples with higher strontium content (x = 0.20), traces of La_2O_3 appear after sintering at higher temperatures (1300 °C to 1500 °C). In samples containing calcium (x = 0 to 0.15), no particular calcium or strontium secondary phases were found after sintering at 1200 °C and also at higher sintering temperatures. In samples with calcium, the presence of secondary phases was negligible after the sintering at 1200 °C, which makes compositions in which strontium is partly substituted with calcium favourable in comparison to compositions containing magnesium or barium.

One of the crucial tasks in the preparation of complex oxide material as an anode in high-temperature fuel cells is to achieve good connections among solid perovskite grains without the appearance of secondary phases. At the same time, pores in the electrode should be continuous. Consistent with the results of powder diffraction in samples containing magnesium and barium grains of secondary phases based on magnesium and barium were observed in the microstructure after sintering at 1200 °C and above (**Figure 3**). In Mg-containing samples, smaller dark grains were ascribed to Mg-Mn and/or Mn-Cr phase, while larger bright grains were ascribed to perovskite. After sintering at 1500 °C, perovskite grains formed dense regions with inclusions of secondary phases. In Ba-containing samples after sintering at 1200 °C, a secondary liquid phase was present between light grey perovskite round grains, while after sintering at 1500 °C the morphology of perovskite grains is changed significantly. The microstructure of sintered samples consists mainly of cubic grains, surrounded by a thin layer of secondary liquid phase, as it was described in the literature for the case of $La_{0.7}Ba_{0.3}Cr_{0.5}Mn_{0.5}O_{3-\delta}$ after sintering at 1650 °C for five hours in air.[28]

The microstructures of the samples in which strontium is partly replaced with calcium (Ca10Sr15 and

Ca15Cr10) after sintering at temperatures from 1200 °C to 1500 °C are presented in **Figure 4**. These samples were selected since no secondary crystal phases were identified by X-ray analysis after sintering at 1200 °C. After sintering at 1200 °C for both samples, a homogenous microstructure was formed in which grains were well connected to each other. At the same time, pores are uniformly distributed in the microstructure and remain opened to the surface allowing gaseous reactants to enter and product to leave the reaction site at the potential anode. After sintering at 1300 °C, porosity is apparently reduced, and pores started to close. In Ca10Sr15 after heating at 1400 °C, inhomogeneous microstructures with dense areas of fine grains and dense areas of coarse grains together with separate large pores can be observed. In sample Ca15Sr10 the size of the grains is much more uniform, and the sample is rather dense. After sintering at 1500 °C, the microstructure of Ca10Sr15 consisted of large grains and some pores at grain borders, while sample Ca15Sr10 is fully dense and some small grains of the secondary phase are present. From these observations, it may be assumed that Sr substitution with Ca to some amount (x = 0.10, 0.15) accelerates sintering at lower temperatures (1200 °C), due to the low-temperature liquid phase formation. Adding Ca to perovskite above or below certain concentrations (x = 0, 0.05, 0.20 and 0.25) does not work on the densifying process in the same way. It is expected that in mixed CaO-SrO-Cr_2O_3 system liquid phase forms at lower temperatures than in specific CaO-Cr_2O_3 [29] and SrO-Cr_2O_3 [19] systems.

Quantitative analysis of microstructures in all sintered samples after sintering was also performed, while only those results of samples containing calcium are summarized in **Table 2**. Parameters d_{max}, d_{min}, ψ and $\overline{d}$ are represented as maximum and minimum intercept lengths in one direction, shape factor, and the diameter of the area-analogue circle, respectively.

As expected, the green density of the samples containing Ca is decreasing with a gradual strontium replacement at the A site in the perovskite, since calcium has a lower molecular mass than strontium. Sintered density depends greatly on the strontium substitution with calcium as well as the sintering temperature. The highest density (3.00 g cm^{-3}) after sintering at 1200 °C achieved sample with medium calcium content (Ca15Sr10), while at the densification process of this sample is not so pronounced higher sintering temperatures. After sintering at temperatures above 1200 °C, the sintered density increases faster in samples with strontium content higher than calcium. Thus, in samples (x = 0.15 and 0.20), after sintering at 1300 °C and 1400 °C, considerable increase in density was noticed. After sintering at 1500 °C in samples containing both calcium and strontium (x = 0 to 0.20). densities are rather high, and they are increasing with strontium content (from 6.26 g cm^{-3} to 6.65 g cm^{-3}). Exceptions are the samples with no Ca (Ca25Sr0) or no Sr (Sr25), where intensive densification starts as high as 1500 °C, meaning that liquid phase, which is formed in the specific systems of CaO-Cr_2O_3 and SrO-Cr_2O_3, does not accelerate sintering. Thus, final densities reached in Ca25Sr0 or Sr25 are only 5.43 g cm^{-3} and 6.10 g cm^{-3}, respectively.

Table 2: Average values selected microstructure parameters, green and sintering density for $La_{0,75}Ca_xSr_yCr_{0,5}Mn_{0,5}O_3$ sintered at 1200 °C, 1300 °C, 1400 °C, and 1500 °C.

	sample	d_{max} / μm	d_{min} / μm	N_{grains}	S_{grain} / μm^2	d / μm	Ψ	ρ_{sinter} / g cm^{-3}
1200 °C	Ca25Sr0	0.90	0.02	2223	0.09	0.31	0.80	2.21
	Ca20Sr5	0.67	0.02	3290	0.05	0.23	0.82	2.45
	Ca15Sr10	0.56	0.01	1736	0.04	0.20	0.82	3.00
	Ca10Sr15	0.60	0.01	1097	0.04	0.21	0.82	2.70
	Ca5Sr20	0.82	0.01	1018	0.07	0.27	0.80	2.74
	Ca0Sr25	0.47	0.01	1419	0.01	0.10	0.83	2.55
1300 °C	Ca25Sr0	1.11	0.02	1455	0.14	0.41	0.81	2.72
	Ca20Sr5	0.99	0.01	677	0.13	0.37	0.79	3.27
	Ca15Sr10	0.85	0.01	351	0.14	0.39	0.82	3.80
	Ca10Sr15	0.86	0.01	143	0.15	0.39	0.81	4.11
	Ca5Sr20	1.52	0.02	500	0.41	0.62	0.81	4.47
	Ca0Sr25	0.76	0.01	291	0.07	0.26	0.80	3.40
1400 °C	Ca25Sr0	1.42	0.02	525	0.33	0.57	0.82	3.59
	Ca20Sr5	1.35	0.01	183	0.28	0.51	0.80	3.63
	Ca15Sr10	1.73	0.02	756	0.38	0.62	0.81	5.26
	Ca10Sr15	2.19	0.02	395	0.69	0.80	0.81	6.18
	Ca5Sr20	3.28	0.03	340	1.66	1.23	0.82	6.68
	Ca0Sr25	1.37	0.01	414	0.25	0.46	0.68	3.89
1500 °C	Ca25Sr0	3.02	0.02	195	1.12	1.03	0.81	5.43
	Ca20Sr5	2.50	0.01	72	0.80	0.81	0.78	6.26
	Ca15Sr10	2.55	0.02	42	2.01	1.27	0.77	6.57
	Ca10Sr15	2.65	0.03	36	2.07	1.25	0.80	6.60
	Ca5Sr20	3.74	0.03	330	2.09	1.36	0.77	6.65
	Ca0Sr25	1.75	0.01	80	0.49	0.53	0.84	6.10

Results of the quantitative microstructural analysis are in good agreement with optical observations. Sintered density increases and optically determined porosity decreases with the increasing sintering temperature. After sintering at 1200 °C samples Ca20Sr5, Ca15Sr10, Ca10Sr15, and Ca5Sr20 also form relatively small average grain sizes of 0.23, 0.20 μm, 0.21 μm 0.27 μm, respectively. The fine-grained microstructure is favourable for ensuring good catalytic activity of the electrode.

Partial strontium substitution with calcium in samples with x = 0.05 to 0.20 resulted in moderate average grain growth from 0.20 μm to 1.36 μm. In the sample containing only calcium Ca25Sr0, average grain size grows from 0.31 μm to 1.03 μm and in the sample with no calcium Sr25 grains grow from 0.10 μm to 0.53 μm. From these data, we may assume that only Sr or Ca additions to LCM perovskite do not accelerate sintering to a level as in the case in which both elements Ca and Sr are added. According to the phase diagram, the SrO–Cr_2O_3 secondary phase $SrCrO_4$ forms a liquid phase

due to eutectic and peritectic reactions that promote sintering, but only by adding Sr to perovskite under certain concentration $x = 0.20$.[19,30] The Sr_2CrO_4-rich phase presence in the *as prepared* materials was confirmed in samples with higher Sr content ($x = 0.15$, 0.20 and 0.25), which at higher temperatures first turns to $SrCrO_4$ and later forms a liquid phase to promote perovskite sintering.[20] With noticeable grain growth, the slightly decreased shape factor Ψ indicates that grains become diverse to ideal spheres, as already observed in the case of combustion-derived LSCM ceramics.[21]

4 CONCLUSIONS

$La_{0.75}Sr_xA_{1-x}Mn_{0.5}Cr_{0.5}O_3$ perovskite materials in which Sr was replaced with alkali earth ions Mg, Ca and Ba ($x = 0$ to 0.25) were prepared using citrate-nitrate combustion synthesis. The solid residue in the as-synthesized samples contains the main perovskite phase with some minor additions of secondary phases (formed carbonates or mixed oxides).

In sintered samples at 1200 °C containing magnesium ($x = 0$ to 0.20), there are two possible secondary phases Mg_2MnO_4 and/or Mn_2CrO_4. These two secondary phases are also present after sintering as high as 1500 °C. In samples containing barium (x = 0 to 0.10), the secondary phases $BaMnO_4$ and $BaCrO_4$ are found, indicating their relatively poor solubility in $LaCrO_3$. In Ca-doped samples in which calcium content is higher than strontium ($x = 0.05$ to 0.10), the presence of secondary phases after the sintering was negligible. This makes Ca-doped LSCM compositions favourable, in comparison to Mg-doped or Ba-doped LSCMs.

After sintering at 1200 °C in Ca-doped LSCMs, relatively small grains of the main perovskite phase are formed. At the same time, the LSCCM phase is continuous, and the pores remain open to the surface. Higher sintering temperatures increase average grain sizes; however, no grains of secondary phases may be found in the materials' macrostructure. In contrast, sintered Ba-doped or Mg-doped LSCMs always contain undesired secondary phases at the grain boundaries between main perovskite grains.

Acknowledgment

We thank for the financial support of the Ministry of Higher Education, Science and Technology of the Republic of Slovenia through grants P1–0175.

5 REFERENCES

[1] J. D. Larminie, Fuel Cell Systems Explained, 2nd Edition. 2nd ed. John Wiley & Sons, Chichester 2003

[2] Rand DAJ, Dell RM. Hydrogen energy: challenges and prospects, RSC Publishing, Cambridge 2008

[3] S. C. Singhal, K. Kendall, High-temperature solid oxide fuel cells: fundamentals, design, and applicatons. Elsevier Advanced Technology, New York 2003

[4] A. Atkinson, S. Barnett, R. J.Gorte, J. T. D. Irvine, A. J. McEvoy, M. Mogensen, S. C. Singhal, J. Vohs, Advanced anodes for high temperature fuel cells, Nat. Mater., 3 (**2004**) 17–24, doi:10.1038/nmat104

[5] H. Hurokawa, T. Z. Sholklaper, C. P. Jacobson, L. C. De Jonghe, S. J. Visco, Ceria nanocoating for sulphur tolerant Ni-based anodes of solid oxide fuel calls, Electrochem.Solid State, 100 (**2007**) 135–138, doi: 10.1149/1.2748630

[6] S. Macintosh, R. J. Gorte, Direct hydrocarbon solid oxide fuel cells, Chem. Rev., 104 (**2004**) 4845-4865, doi:10.1021/cr020725g

[7] C. Sun, U. Stimming, Recent anode advances in solid oxide fuel cells, J. Pow. Sources, 171 (**2007**) 247–260, doi:10.1016/j.jpowsour.2007.06.086

[8] S. P. Jiang, L. Liu, K. O. Ong, P. Wu, J. Li, J. Pu, Electrical conductivity and performance of doped $LaCrO_3$ perovskite oxides for solid oxide fuel cells, J. Power. Sources, 176 (**2008**) 82, doi:10.1016/j.jpowsour.2007.10.053

[9] K. O. Ong, P. Wu, J. Li, S. P. Jiang, L. Liu, Optimization of electrical conductivity of $LaCrO_3$ through doping: A combined study of molecular modeling and experiment, Appl. Phys. Lett., 90 (**2007**), doi:10.1063/1.2431780

[10] R. Koc, H.U. Anderson, Electrical conductivity and Seebeck coefficient of (La, Ca) (Cr, Co)O_3, J. Mater. Sci., 27 (**1992**), 5477–5482, doi: 10.1007/BF00541609

[11] J. Yoo, A. Verma, A. J. Jacobson, T. A. Ramanarayanan (Ed.), Ionic and Mixed Conducting Ceramics IV, The Electrochemical Society Inc., 2001, 27

[12] L. Deleebeeck, J. L. Fournier, V. Birss, Comparison of Sr-doped and Sr-free $La_{1-x}Sr_xMn_{0.5}Cr_{0.5}O_{3\pm\delta}$ SOFC Anodes, Solid State Ionics, 181 (**2010**) 1229-1237, doi:10.1016/j.ssi.2010.05.027

[13] L. Deleebeeck, J. L. Fournier, V. Birss, Catalysis of the hydrogen oxidation reactions by Sr-doped $LaMn_{1-y}Cr_yO_{3\pm\delta}$ oxides, Solid State Ionics, 203 (**2011**), 69-79

[14] S. Tao, J. T. S. Irvine, Synthesis and characterization of $La_{0.75}Sr_{0.25}Cr_{0.5}Mn_{0.5}O_{3-\delta}$ a redox stable, efficient perovskite anode for SOFCs, J. Electrochem. Soc., 151 (**2004**) 252–259, doi:10.1149/1.1639161

[15] J. Wan, J. H. Zhu, J. B. Goodenough, $La_{0.75}Sr_{0.25}Cr_{0.5}Mn_{0.5}O_{3-\delta}$ + Cu composite anode running on H_2 and CH_4 fuels, Solid State Ionics, 177 (**2006**), 1211–121, doi:10.1016/j.ssi.2006.04.046

[16] S. P. Jiang, L. Zhang, Y. Zhang, Lanthanum strontium manganese chromite cathode and anode synthesized by gel-casting for solid oxide fuel cells, J. Mater. Chem., 17 (**2007**), 2627–2635, doi:10.1039/ b701339f

[17] R. Pelosato, C. Cristiani, G. Dotelli, M. Mariani, A. Donazzi, I. N. Sora, Co-precipitation synthesis of SOFC electrode materials, Int. J. Hydrogen Energ., 38 (**2013**), 480–491, doi:10.1016/j.ijhydene.2012.09.063

[18] B. H. Sang, C. Pyeong-Seok, H. C. Yoon, L. Dokyol, L. Jong-Heun, Preparation of $La_{0.75}Sr_{0.25}Cr_{0.5}Mn_{0.5}O_{3-\delta}$ fine powders by carbonate coprecipitation for solid oxide fuel cells, J. Power Sources, 195 (**2010**), 124–129, doi:10.1016/j.jpowsour.2009.06.078

[19] E. M. Levin, H. F. McMurdie, Phase Diagrams for Ceramists, The American Ceramic Society, 1975, 29

[20] P. H. Duvigneaud, Factors Affecting the Sintering and the Electrical Properties of Sr-Doped $LaCrO_3$, J. European Cer. Soc., 14 (**1994**), 359–367, doi:10.1016/0955-2219(94)90073-6

[21] K. Zupan, M. Marinšek, Combustion Derived $La_{1-x}Sr_xMn_{0.5}Cr_{0.5}O_{3\pm\delta}$ (x = 0.20, 0.25) Perovskite: Preparation, Properties, Characterization, Materials and technology, 48 (**2014**), 885–891

[22] M. Marinšek, K. Zupan, J. Maček, Citrate-nitrate gel transformation behavior during the synthesis of combustion-derived NiO-yttria-stabilized zirconia composite, J. Mater. Res., 18 (**2003**), 1551–1560

[23] H. W. Wang, D. A. Hall, F. R. Sale, A thermoanalytical study of the metal nitrate-EDTA precursors for lead zirconate titanate ceramic powders, J. Therm. Anal., 41 (**1994**), 605–620, doi:10.1007/BF02549337

[24] S. T. Aruna, M. Muthuraman, K. C. Patil, Synthesis and properties of Ni-YSZ cermet: anode material for solid oxide fuel cells, Solid State Ionics, 111 (**1998**), 45–51, doi:10.1016/S0167-2738(98)00187-8

[25] M. Marinšek, J. Kemperl, B. Likozar, J. Maček, Temperature Profile Analysis of the Citrate-Nitrate Combustion System, Ind. Eng. Chem. Res., 47 (**2008**), 4379–4386, doi:10.1021/ie800296m

[26] H. Yokohawa, N. Sakai, T. Kawada, M. Dokiya, Chemical Thermodynamic Considerations in Sintering of $LaCrO_3$?-?Based Perovskites, J. Electrochem. Soc. 138 (**1991**), 1018–1027, doi:10.1149/1.2085708

[27] J. H. Ouyang, S. Sasaki, T. Murakami, K. Umeda, Spark-plasma-sintered $ZrO_2(Y_2O_3)$-$BaCrO_4$ self-lubricating composites for high temperature tribological applications, Ceram. Int., 31 (**2005**), 543–553, doi:10.1016/j.ceramint.2004.06.020

[28] L. Zhang, X. Chen, S. P. Jiang, H. Q. He, Y. Xiang, Characterization of doped $La_{0.7}A_{0.3}Cr_{0.5}Mn_{0.5}O_{3-\delta}$ (A=Ca, Sr, Ba) electrodes for solid oxide fuel cells, Solid State Ionics, 180 (**2009**), 1076–1082, doi:10.1016/jssi.2009.05.010

[29] J. P. R. De Villiers, J. Mathias, A. Maun, Phase relations in the System CaO- Cromium Oxide- SiO_2 in Air, and Solid Solution Relations along the Ca_2SiO_4- $Ca_3(CrO_4)_2$ Join, Trans. Inns. Min. Matall, Sect. C, 96 (**1987**), C55–C62

[30] K. Zupan, M. Marinšek, T. Skalar, Phase and microstructure development of LSCM perovskite materials for SOFC anodes prepared by the carbonate-coprecipitation method, Materials and technology, 50 (**2016**), 743–748, doi: 10.17222/mit.2015.232